Available online at www.sciencedirect.com
SCIENCE DIRECT®

Journal of the European Ceramic Society 23 (2003) 2821–2828

www.elsevier.com/locate/jeurceramsoc

Ceramic–metal interaction and wetting phenomena in the B_4C/Cu system

N. Froumin*, N. Frage, M. Aizenshtein, M.P. Dariel

Ben-Gurion University of the Negev, Beer-Sheva, Israel

Abstract

The experimental study of the wetting phenomena in the boron carbide–copper system, using the sessile drop method at 1150 °C shows that molten Cu attacks boron carbide substrates forming a crater below the contact area. Boron additions prevent crater formation, improve wetting and, for a 10 at.% B alloy, reduce the equilibrium wetting angle to 40°. Thermodynamic analysis of the Cu–B–C system in the Cu-rich corner confirms the experimental results. These results and similar ones obtained in the TiC–Cu system suggest that the presence of a carbide phase over a concentration range is a key feature that governs wetting phenomena and chemical interaction at these metal–carbide interfaces.

Keywords: Boron carbide; Copper; Interface; Phase diagram; Wetting

1. Introduction

Boron carbide and boron carbide-based cermets are promising materials for a variety of applications that require elevated hardness values, good wear and corrosion resistance. Interfacial properties directly affect the processing of metal–ceramic composites and, in particular, the brazing of ceramic parts has attracted a great deal of interest. Naidich[1] established that for metals with a weak affinity to B and C, such as Cu, Ag, Au and Sn (the so called non-reactive metals), the values of the contact angle on B_4C fall in the range of 130–140°. Similar values of the contact angles were reported by.[2] In these studies, however, the wetting behavior of alloys based on the non-reactive metals and the structure of the interface have not been fully investigated as a function of the alloy composition.

Preliminary experiments have confirmed the apparently non-wetting behavior of molten Cu in contact with boron carbide substrates. Paradoxically, however, careful examination revealed that the molten metal attacked the substrate forming a crater below the contact area (Fig. 1). This apparent inconsistency impelled us to undertake an in-depth examination of the wetting in the B_4C–Cu system that included a detailed thermodynamic analysis of the Cu-rich corner of the ternary Cu–B–C system. The results of the analysis suggested that the boron content of the molten alloy is a dominant parameter that determines the wetting behavior in this system. Experimental evidence based on sessile drop measurements and structural examination fully confirmed these predictions.

2. Thermodynamic analysis

The phase equilibria in the ternary Cu–B–C system is based on the corresponding binary B–C, Cu–C and Cu–B systems at 1200 °C, shown in Figs. 2–4. The boron carbide phase extends over a wide composition range from B_4C to $B_{10}C$ (Fig. 2).[3] Boron carbide with higher carbon content is in equilibrium with graphite, while the boron rich side of the carbide phase is in equilibrium with pure boron. The solubility of carbon in liquid copper at 1200 °C is very low [$x_C^* < 5 \cdot 10^{-7}$atomic fraction][4] and no carbide phase is present in the Cu–C system (Fig. 3). The Cu–B system displays a eutectic at 13.3 at.% and 1013 °C, at 1200 °C the solubility of Cu in solid B is about 3–4 at.% and that of boron in liquid Cu is about 27 at.% (Fig. 4).[5] Since no stable ternary

* Corresponding author. Tel.: +972-7-646-1475; fax: +972-7-947-2946.

E-mail address: nfrum@bgumail.bgu.ac.il (N. Froumin).

0955-2219/03/$ - see front matter © 2003 Elsevier Ltd. All rights reserved.
doi:10.1016/S0955-2219(03)00294-2

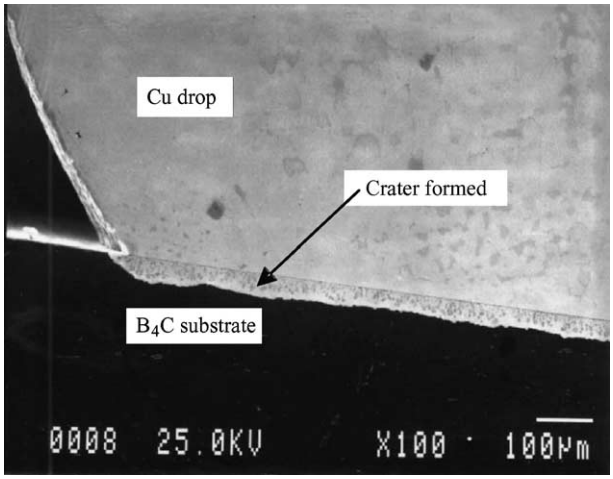

Fig. 1. Cross-section of the interface between unalloyed Cu drop and boron carbide. Notice the high contact angle and the crater formation.

phase in the Cu–B–C system has been reported, an isothermal section for this system may be constructed, as shown in Fig. 5.

In Fig. 5, the phase equilibrium regions are denoted by the Roman numbers: I-single phase region of the Cu–B–C liquid solution (L.S.), II-two-phase region of L.S. with boron carbide of various compositions, III-L.S.+ graphite, IV-three-phase region with L.S., corresponding to point O_1, + graphite + B_4C, V-L.S., corresponding to point O_2, + $B_{10}C$ + boron, saturated with Cu, VI-solid B–Cu solution + $B_{10}C$, VII-two-phase region with L.S., corresponding to point O_2, + boron, saturated with Cu.

The dotted line 1 corresponds to the situation according to which stoichiometric boron carbide and pure copper are taken as starting materials for the wetting experiments. This line crosses regions III and IV in which graphite is the stable phase, consequently, free carbon may form at the metal–ceramic interface. Line 2, corresponds to the situation in which an initial Cu–B solution is in contact with stoichiometric boron carbide. Since, according to the phase diagram, this is a non-equilibrium situation, the system will strive by dissociation of boron carbide to reach a stable equilibrium corresponding to the tie lines in the two-phase II region. This two-phase region consists of a liquid Cu–B alloy and substoichiometric boron carbide. Notice that in this case no free carbon is expected and, therefore, by starting with an appropriate composition of Cu–B liquid solution, it is possible to prevent graphite precipitation on the metal–ceramic interface and, thereby, alter the wetting conditions. The initial boron content in the liquid Cu, must however, be higher than that corresponding to point O_1.

It is of obvious interest to determine the coordinates of the O_1–O_2 line and the compositions of the corresponding boron carbide phase. This may be done by taking into account the thermodynamic properties (chemical potential, μ_1) of the components in the Cu–B–C liquid solution and of boron and carbon in the nonstoichiometric carbide phase. At equilibrium, the chemical potentials of the components:

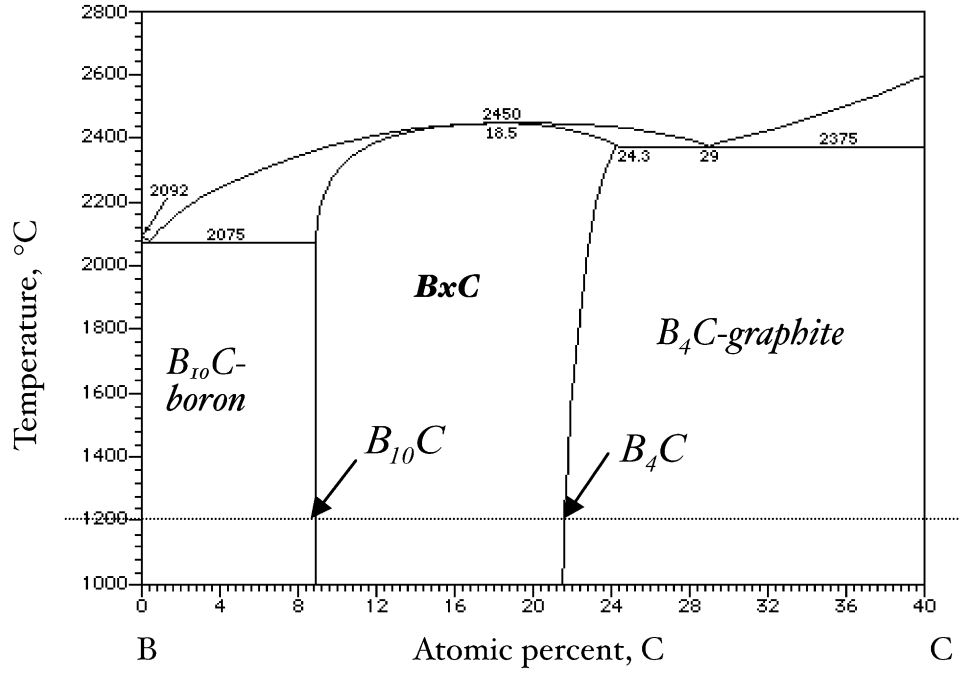

Fig. 2. The boron–carbon phase diagram.

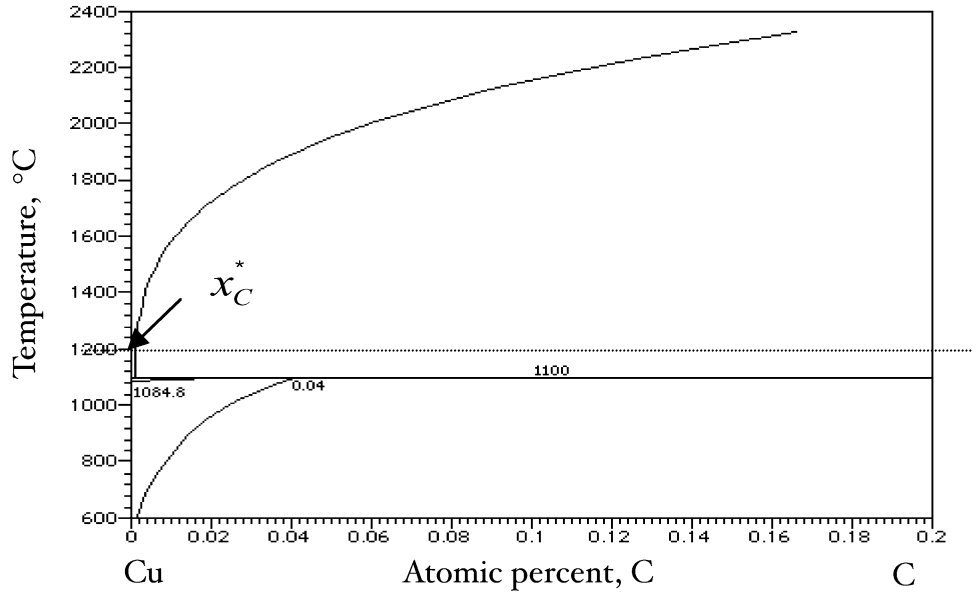

Fig. 3. The copper–carbon phase diagram.

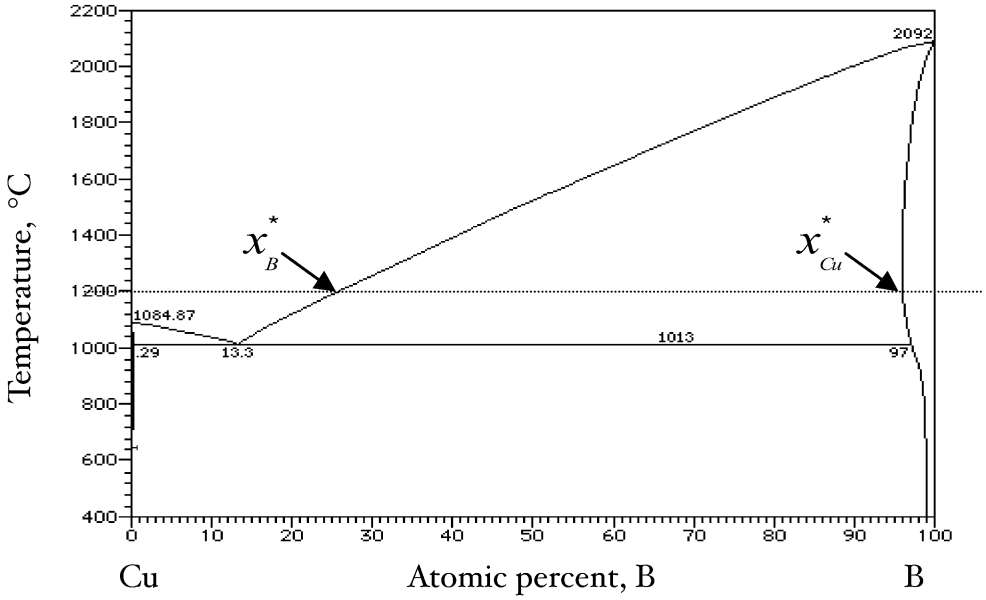

Fig. 4. The copper–boron phase diagram.

$$\mu_B(\text{liquid}) = \mu_B(\text{carbide}),\ \ \mu_C(\text{liquid}) = \mu_C(\text{carbide}) \quad (1)$$

First consider the properties of the Cu–B–C liquid solution. The solubility of carbon is extremely low and its effect on the B activity in the ternary liquid solution may be neglected. The thermodynamic properties of the Cu–B binary liquid solution were investigated by Batalin et al.[6] at 1790 K. A positive departure from ideality was observed and the values of the boron partial mixing enthalpy $\Delta\bar{H}_B$ were reported for the 0–9 at.% boron concentration range. The value of $\Delta\bar{H}_B^o = 20$ kJ/mol for an infinite dilute solution was derived from the reported data for 1473 K, according to a regular solution approach. Thus the boron chemical potential in dilute solution may be expressed by Eq. (2)

$$\mu_B(\text{liquid}) = \mu_B^0(\text{liquid}) + RT\ln x_B + \frac{\Delta\bar{H}_B^0}{RT}, \quad (2)$$

where μ_B^0(liquid)—the chemical potential of pure liquid boron, x_B—boron atomic fraction in the liquid.

Since the carbon concentration in the liquid solution is extremely low we will operate with carbon activity

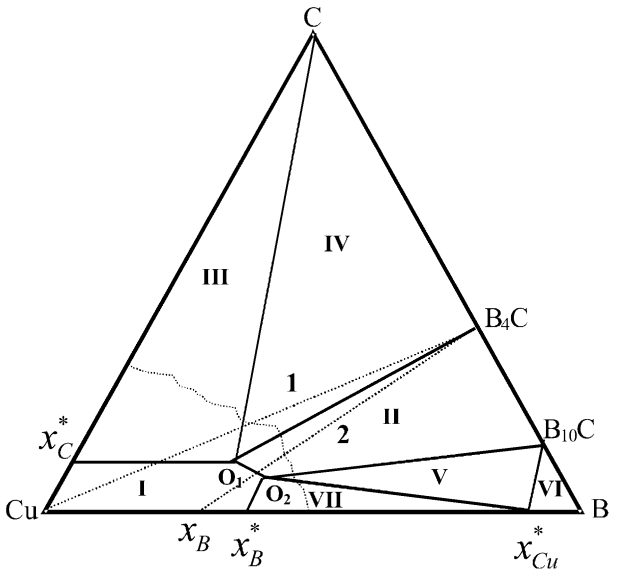

Fig. 5. Schematical isothermal section at 1200 °C of the ternary Cu–B–C phase diagram. The Cu-rich corner is out of scale.

(a_C) only, thus for the carbon chemical potential we have

$$\mu_C(\text{liquid}) = \mu_C^0(\text{graphite}) + RT\ln a_C, \quad (3)$$

where μ_C^0(graphite)—the chemical potential of carbon in its standard state.

The chemical potentials of carbon and boron in the nonstoichiometric boron carbide, according to our previously reported data,[7] may be expressed by Eqs. (4) and (5)

$$\mu_C(\text{carbide}) = \mu_C^0(\text{graphite}) + \ln X_C + \frac{-445000}{RT}\left[(1-X_C)^2 - 0.64\right] + 1.609 \quad (4)$$

$$\mu_B(\text{carbide}) = \mu_B^0(\text{carbide}) + \ln X_B + \frac{-445000}{RT}\left(X_C^2 - 0.0081\right) + 0.0943, \quad (5)$$

where X_B and X_C are the boron and carbon atomic fraction in boron carbide, μ_B^0(carbide)—the chemical potential of pure solid boron. It must be noted that

$$\mu_B^0(\text{liquid}) - \mu_B^0(\text{carbide}) = \Delta G_f^0 = \Delta H_f^0 - T\frac{\Delta H_f^0}{T_f} = 22175 - 9.64T, \quad \text{J/mol}, \quad (6)$$

where ΔG_f^0, ΔH_f^0 and T_f are the Gibbs energy, the melting enthalpy and temperature of boron, were taken from Ref. 8.

Combining Eqs. (1)–(6) the equilibrium compositions of the liquid solution and the carbide phase were calculated and are shown in Fig. 6.

According to these thermodynamic calculations the boron content at point O_1 corresponding to the equilibrium between a carbon saturated liquid solution ($a_C = 1$) and stoichiometric boron carbide is about 3.4 at.% . The boron carbide phase with a composition that corresponds to $B_{10}C$ is in equilibrium with a liquid solution containing about 25 at.% boron (point O_2). As can be seen from the calculated diagram, that dotted line 1, which links the Cu corner with the point corresponding to B_4C, crosses regions III and IV and graphite may precipitate during the interaction at the interface. However, any line linking a liquid Cu–B solution, with a boron content higher than 3.4 at.%, (dotted line in Fig. 6) to stoichiometric B_4C, will not cross the graphite containing regions and, therefore, graphite precipitation during the metal–ceramic interaction is prevented. In that case, the original conditions at the metal–ceramic interface are maintained and any subsequent variations of the equilibrium contact angle may be attributed to subtle altering of the near-surface layer composition of the boron carbide substrate.

In order to check the validity of the thermodynamic analysis, we undertook an experimental study that included wetting experiments couples with structural analysis by optical and scanning electron microscopy and AES depth profiling.

3. Experimental procedures

The B_4C ceramic samples with near-theoretical density were obtained from hot-pressed powder with particle size 1–3 μm (Starck). The substrate surfaces for wetting experiments were polished down to the 0.25 μm diamond paste level and gently cleaned in acetone and alcohol in an ultrasonic bath. A Cu–master alloy (11 at.%B) was prepared from Cu (99.999% purity) and B powder (99.90 purity) in an arc furnace. The other

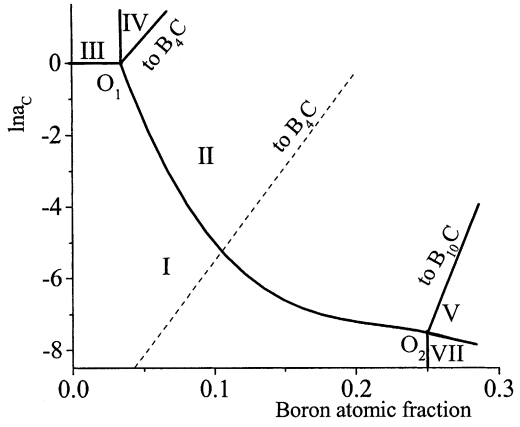

Fig. 6. The Cu-rich corner in the calculated isothermal section of the ternary Cu–B–C phase diagram at 1200 °C. The Roman numerals design the same equilibrium regions as in Fig. 5. Due to the logarithmic scale of the carbon activity axis, the dashed line is out of scale.

alloys were prepared by in-situ co-melting Cu with an appropriate amount of the master alloy.

Wetting experiments were performed using the sessile drop technique at 1150 °C in a vacuum furnace (10^{-3} Pa) described elsewhere.[9] Contact angles were measured directly from the magnified profile images of the molten metal drop in the 5-min time interval up to 60 min of contact. The structure of the interface layer was studied from the cross-section of the solidified drops. The interface composition was determined by EPMA/EDS analysis.

4. Experimental results

4.1. Wetting phenomena

A high non-wetting contact angle close to 110° was observed for Cu on the B_4C substrate. This value was determined after the first 10 min and did not change during the 60 min of contact time (Fig. 7). The wetting angle of the boron containing alloys varied as a function of the contact time (Fig. 7) and reached after 40 min, equilibrium values that decreased with increasing boron content (Fig. 8).

4.2. Interface structure and composition

A recurring feature of this metal–ceramic interface is the formation of a crater in the ceramic substrate due to the strong interaction of the molten Cu drop with boron carbide, a cross-section of which is shown in Fig. 9. Line scan analysis (Fig. 10) allowed to identify the dark spots in the crater as carbon-rich areas and the gray intergranular phase in the copper as boron that precipitated during the solidification of the copper drop. The chemical composition, determined at points 1, 2 and 3 (Fig. 10, Table 1) as well as the element mapping (Fig. 11) confirm the results of the line scan analysis.

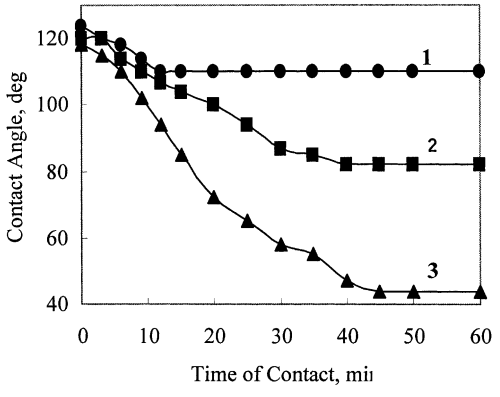

Fig. 7. The contact angles of the Cu–B alloys on B_4C substrates as a function of the contact time at 1150 °C: (1: Cu; 2: Cu-6.2 at.% B; 3: Cu-10.7 at.% B).

These results are in agreement with the thermodynamic analysis predicting for unalloyed copper in contact with boron carbide the dissociation of the carbide accompanied by carbon precipitation as graphite and boron dissolution in the melt. The cross-section of the interface of boron carbide with a 10.7 at% B is shown in Fig. 12. In this system, the interface stays smooth without any evidence of crater formation.

According to the thermodynamic analysis, the equilibrium at the interface is established between the boron-containing copper alloy and a non-stoichiometric boron carbide. A change in the composition of the near surface region of the boron carbide substrate was consequently expected. Any such change would occur only in a very narrow near-surface region due to the limited mass-transport that takes place in boron carbide at 1200 °C. After removal of the metal drop from the substrate, the compositional change within the near surface layer of the carbide was determined by AES depth profiling.

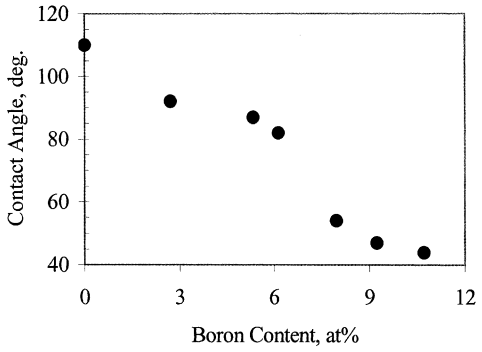

Fig. 8. The equilibrium contact angle of the Cu–B alloys on the B_4C substrate at 1150 °C.

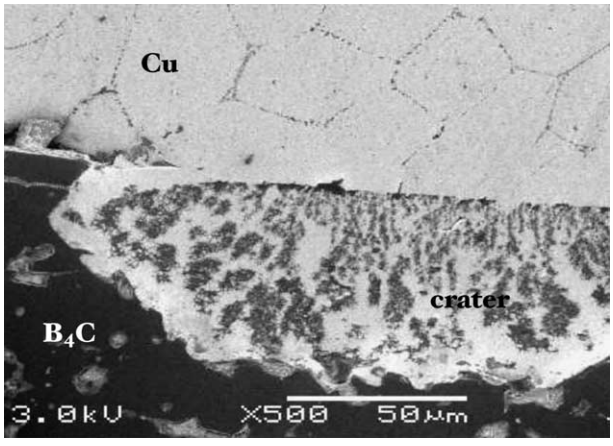

Fig. 9. Cross-section of the interface between initially unalloyed Cu on boron carbide. Notice the deep crater formed below the copper drop. The dark areas within the crater are graphite particles imbedded in the copper–boron alloy. During solidification, excess boron in the molten alloy, precipitated at the copper grain boundaries.

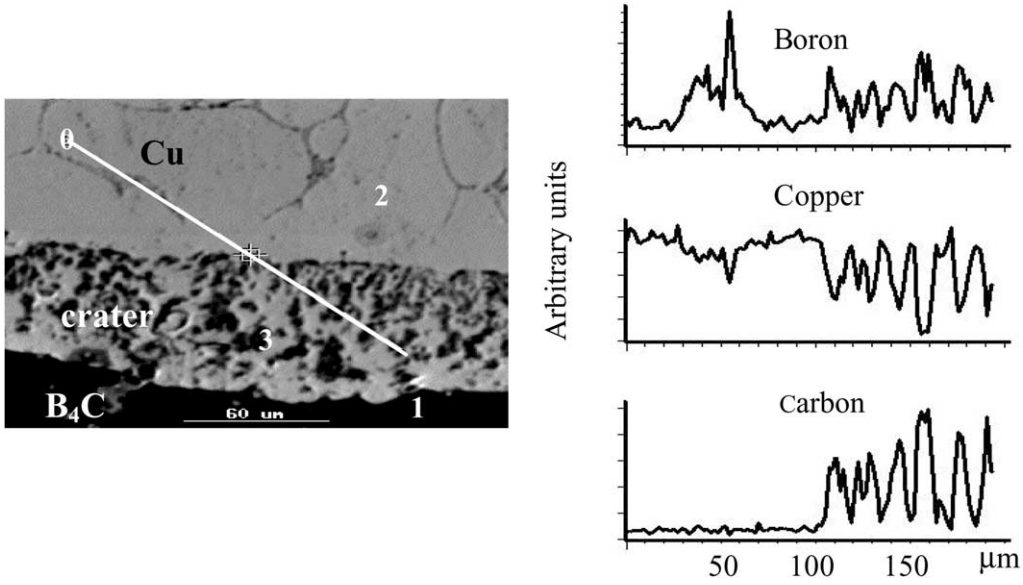

Fig. 10. Line scans of the Cu, B and C across the metal–ceramic interface.

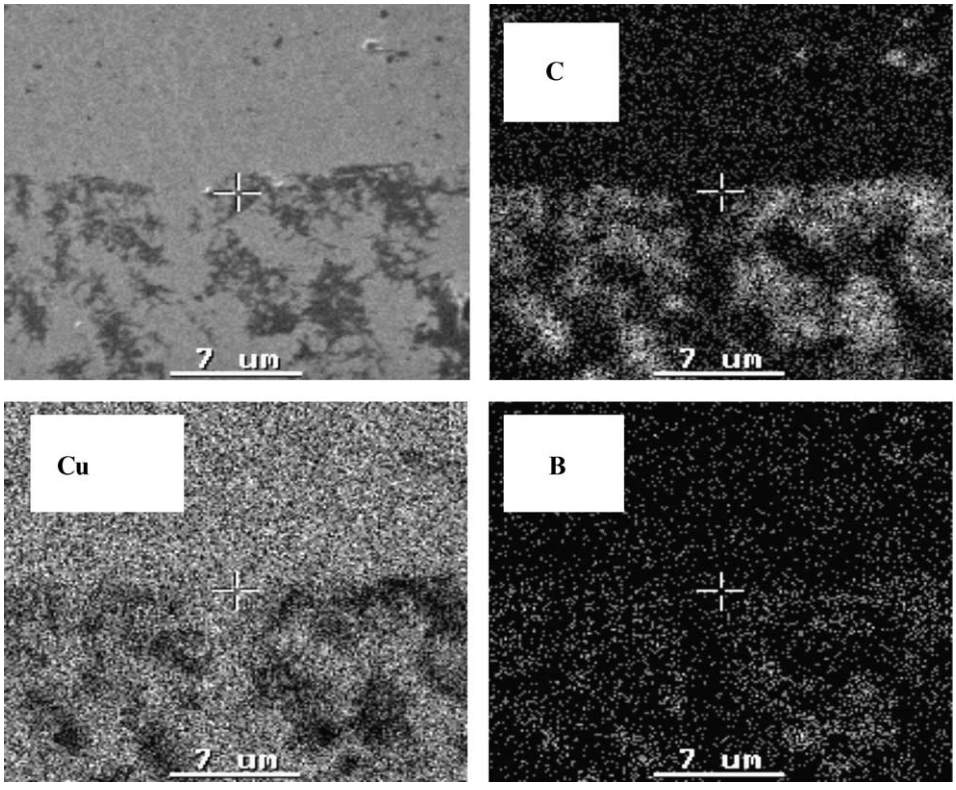

Fig. 11. Surface mapping of C, Cu and B at the cross-section of the boron carbide–Cu interface.

The results expressed by the B/C ratio profile as a function of sputtering time, i.e. depth below the surface is shown in (Fig. 13). The B/C ratio near the surface layer is substantially higher than at a free surface or in the bulk material.

5. Discussion

The results of the thermodynamic analysis are in good agreement with the experimental results. The formation of the crater in the boron carbide substrate may be

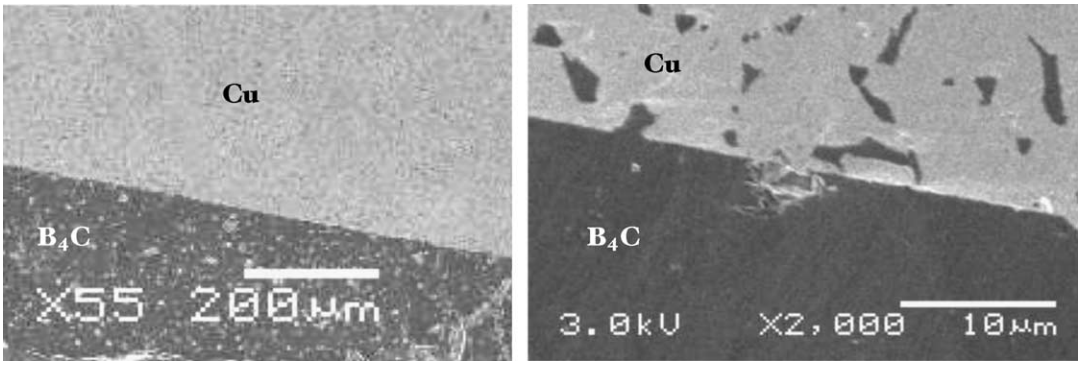

Fig. 12. Cross-section of the interface between boron carbide and a Cu–B 2.8 at.% alloy at two different magnifications.

Table 1
Chemical composition of different points (see Fig. 10) close to the metal-ceramic interface

Point	Composition, at.%		
	B	C	Cu
1 (B_4C)	77	23	0
2 (Cu)	3	97	0
3 (crater)	2.1	11.7	86.2

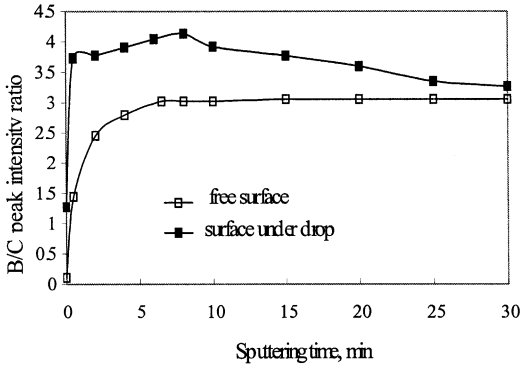

Fig. 13. Depth profiling of the boron-to-carbon ratio within the near surface layer of boron carbide, starting (1) under the interface with a copper drop; (2) at a copper free ceramic surface. The sputtering rate was ~3nm/min.

attributed to the dissociation of the carbide in contact with unalloyed copper. Boron that is released dissolves in the whole volume of the liquid metal. Some of the carbon released from the carbide forms agglomerates dispersed in the molten metal contained within the volume of the crater and some of it is left as a surface carbon layer. The presence of this layer prevents wetting of the solid. Similar effects were observed in the SiC–Cu system.[10,11] In contrast, the interface between boron carbide and a Cu(B) alloys with as little as 3 at.% B, remained smooth and no evidence of any graphite precipitation was observed. This case evidently corresponds to the dotted line 2 in Fig. 12. The altering of the boron carbide composition in the near-surface region close to the interface with liquid Cu–B melt is an additional confirmation of the validity of the thermodynamic analysis. Similar interface phenomena were observed in the TiC_x-Cu system, in which changes of the substrate composition, within the stoichiometric range of the titanium carbide phase, and the wetting behavior were affected by Ti additions to liquid Cu.[12] Apparently, the presence of a concentration range of the carbide phase is a key feature, which governs the wetting phenomena and the chemical interaction on these metal–carbide interfaces.

6. Conclusions

In spite of the commonly accepted non-reactive and non-wetting behavior of boron carbide by molten copper, the latter attacks boron carbide substrates forming a crater below the contact area. Thermodynamic analysis of the Cu–B–C system in the Cu-rich corner suggests that boron additions to molten Cu should eliminate the disruption of the boron carbide. The experimental study of the wetting phenomena in the boron carbide–copper system, using the sessile drop method at 1150 °C, confirmed the results of the thermodynamic analysis. Boron additions prevent crater formation, improve wetting and, for a 10 at.% B alloy, reduce the equilibrium wetting angle to 40°. These results and similar ones obtained in the TiC–Cu system suggest that the presence of a carbide phase over a concentration range is a key feature that governs wetting phenomena and chemical interaction at these metal–carbide interfaces.

Acknowledgements

This work was supported by the Israeli Ministry of Science within the framework of Project No. 20562-01-99.

References

1. Naidich, Ju.V., The wettability of solids by liquid metals. Prog. *Surf. Membr. Sci*., 1981, **14**, 353–484.
2. Kennedy, A. R., Wood, J .D. and Weager, B. M., *The wetting and spontaneous infiltration of ceramics by molten copper*. *J. Mater. Sci*., 2000, **35**, 2909–2912.
3. Thevenot, F., Boron carbide—a comprehensive review. *J. European Ceram. Society*, 1990, **6**, 205–225.
4. Oden, L. L. and Gokcen, N. A., Cu–C and Al–Cu–C phase diagrams and thermodynamic properties of C in the alloys from degrees C to 2300 degrees C. *Metall. Trans*, 1992, **1550**, 23 B, 453-458.
5. Massalski, T. B., Subramanian, P. R., Okamoto, H. and Kacprazak, L., *Binary alloy phase diagrams*, 2nd edn. ASM International, Materials Park, OH, 1990.
6. Batalin, G. I., Sudavtsova, V. S. and Mikhailovskaya, M. V., Thermodynamic properties of molten copper-boron alloys. *Izv. Vyssh. Uchebn. Zaved., Tsvetn. Metall*, 1985, **2**, 125–127.
7. Levin, L., Frage, N. and Dariel, M. P., The effect of Ti and TiO_2 addition on the pressureless sintering of B_4C. *Metall. Mater. Trans*, 1999, **30A**, 3201–3210.
8. Glushko, V., Gurvich, J., ed., *Thermodynamic Properties of the Individual Substances, Vol. 3*. VINITI, Moscow, 1981.
9. Froumin, N., Frage, N., Polak, M. and Dariel, M.P., *Wettability and phase formation in the TiC_x/Al systems*. *Scripta Metal*, 1997, **37**, 1263–1266.
10. Rado, C., Drevet, B. and Eustathopoulos, N., The role of compound formation in reactive vetting: the Cu/SiC system. *Acta Mater*., 2000, **48**, 4483–4491.
11. Xiao, P. and Derby, B., Wetting of silicon carbide by chromium containing alloys. *Acta Mater*., 1998, **46**, 3491–3499.
12. Frage, N., Froumin, N. and Dariel, M. P., Wetting of TiC by non-reactive liquid metals. *Acta Mater*., 2002, **2**, 237–245.